Dynamics of light transmission in two-dimensional nonlinear optical superlattices

Bin Xu* and Nai-Ben Ming
National Laboratory of Solid State Microstructures, Nanjing University, Nanjing 210008, People's Republic of China
(Received 22 April 1994)

A set of coupled-mode equations is developed to describe the multiwave diffraction of light in two-dimensional nonlinear superlattices, and is solved by numerical methods. At low incident intensities, the solution is time-independent and shows that bistable behavior may appear in the incident-diffracted relations. With an increasing incident intensity, the solution becomes unstable and eventually turns chaotic through the route of intermittance. The threshold intensity for chaos varies with the index-modulation strengths of the superlattice. If the relaxation time of the Kerr-form nonlinearity exceeds the transmission time, only stable solutions are obtained.

PACS number(s): 42.50.Ne, 42.25.Fx

I. INTRODUCTION

An optical system with an output as a nonlinear function of some parameter will exhibit bistability in the presence of a positive feedback. Ordinarily, such an optical system will also exhibit unstable or even chaotic behavior under suitable conditions. The Fabry-Pérot étalons filled with nonlinear index media and the hybrid bistable devices are two examples [1].

In recent years, one-dimensional (1D) nonlinear optical superlattices, i.e., nonlinear media with 1D periodic variations in their refractive indices, have been investigated for bistable behavior [2–8]. It has been demonstrated that when the incident intensity is high enough, the transmission becomes unstable and the chaotic behavior appears [9–12]. These phenomena are related to the transition between a forbidden transmission state and an allowed transmission state. In the presence of gap solitons, the propagating wave located in the forbidden gap is brought into the allowed band of the transmission spectrum in a dispersive way [6,12,13] through the Kerr-form dielectric nonlinearity. The changed transmission state will in turn affect the excitation of gap solitons. This kind of interaction may reach a stable state, which can give a bistable behavior, or it may not reach a stable state, in which case instabilities such as chaos will be exhibited [9,11,12].

Recent work by the present authors [14] revealed that in the multiwave diffraction of light in a two-dimensional (2D) nonlinear superlattice (a nonlinear dielectric medium with its refractive index modulated in two dimensions), the incident-diffracted relations may exhibit bistable behavior. Compared with the dispersive mechanism in 1D superlattices, the bistability in 2D cases is established by a different mechanism. It is related to the transition between a low transmission state and a high transmission state in the allowed band, and is not mediated by gap solitons. This transition is not of a dispersive nature but results from the change of index-modulation strengths [14] of the 2D superlattice. The distinction between this kind of bistable mechanism and the dispersive mechanism is clearly stated in Refs. [14] and [15]. In the allowed band, when the index-modulation strengths change, the intensity of each diffracted wave will oscillate between low and high transmission states. Through the Kerr-form nonlinearity, the interference in the transmission field will perturb the index-modulation strengths. Hence a positive feedback is formed. This bistable mechanism, named the index-modulation mechanism, was demonstrated experimentally in our later work in which a photorefractive sample was used to construct the 2D nonlinear superlattice [15]. Unstable phenomena such as self-pulsing were observed in that experiment. In this paper, to supplement our previous work, based on the physical pictures already provided, we investigate the dynamics of light transmission and unstable behavior in a 2D nonlinear superlattice from a detailed numerical approach.

The 2D nonlinear superlattice we consider here is a Kerr-form nonlinear medium with the linear term of its dielectric constant modulated periodically in two dimensions. Its periodicity is expressed by the vectors $\mathbf{H}_x$ and $\mathbf{H}_y$ in reciprocal space. The incident wave vector satisfies the exact Bragg condition that four reciprocal points are located on the Ewald sphere. Thus four diffracted waves are excited in the medium (see Fig. 1). The four waves are coupled with one another not only by the Bragg resonance, but also by the Kerr-form dielectric nonlinearity. In Sec. II we develop a set of first-order partial differential equations in a way similar to the coupled-mode theory to describe the dynamics of light transmission in this 2D superlattice. The relaxation of the dielectric nonlinearity is considered. In Sec. III we use numerical methods to solve the equations and obtain both time-independent and time-dependent solutions. In Sec. IV the results are discussed.

*Present address: Department of Electrical Engineering and Computer Science, Massachusetts Institute of Technology, Cambridge, MA 02139.

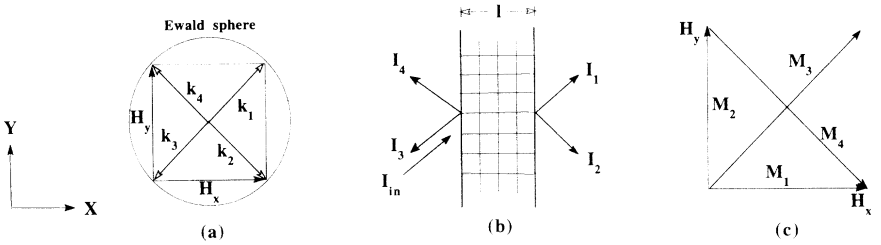

FIG. 1. Four-wave diffraction model in a two-dimensional nonlinear optical superlattice. (a) Bragg condition with four reciprocal points located on the Ewald sphere. $\mathbf{k}_1$ is the incident wave vector; $\mathbf{k}_2$, $\mathbf{k}_3$, and $\mathbf{k}_4$ are wave vectors of the other three diffracted waves. (b) Schematic diagram of four-wave diffraction in real space. (c) Four index-modulation strengths M_1, M_2, M_3, and M_4, as Fourier components of the periodic refractive index along reciprocal vectors $\mathbf{H}_x$, $\mathbf{H}_y$, $\mathbf{H}_x+\mathbf{H}_y$, and $\mathbf{H}_x-\mathbf{H}_y$, respectively.

II. COUPLED-MODE EQUATIONS

Waves propagating in periodic structures take the Bloch-wave formalism. In this model of four-wave diffraction, the light field in the 2D superlattice can be expressed as

$$\mathbf{E}(\mathbf{r},t)=\tfrac{1}{2}e^{i(\mathbf{k}_1\cdot\mathbf{r}-\omega t)}\sum_{i=1}^{4}\mathbf{E}_i e^{i\mathbf{H}_i\cdot\mathbf{r}}+\text{c.c.}$$
$$=\tfrac{1}{2}\sum_{i=1}^{4}\mathbf{E}_i e^{i(\mathbf{k}_i\cdot\mathbf{r}-\omega t)}+\text{c.c.}\ , \tag{1}$$

where $\mathbf{k}_1$ is the incident wave vector [see Fig. 1(a)]. $\mathbf{k}_i$ $(=\mathbf{k}_1+\mathbf{H}_i,\ i=2,3,4)$ are the wave vectors of the other diffracted waves. $\mathbf{H}_i$ are the reciprocal vectors located on the Ewald sphere. $\mathbf{E}_i$ $(i=1,2,3,4)$ are the envelopes of the diffracted waves varying with space and time.

The equation governing the light field is derived from Maxwell's equations in nonlinear media,

$$\nabla\times[\nabla\times\mathbf{E}(\mathbf{r},t)]+\mu_0\epsilon_0\epsilon(\mathbf{r})\frac{\partial^2\mathbf{E}(\mathbf{r},t)}{\partial t^2}=-\mu_0\frac{\partial^2\mathbf{P}_{\mathrm{NL}}(\mathbf{r},t)}{\partial t^2}\ . \tag{2}$$

$\epsilon(\mathbf{r})$ is the linear term of the medium's dielectric constant and is periodic in two dimensions. Thus it can be expanded into the Fourier series along the reciprocal vectors, which are linear combinations of the unit reciprocal vectors $\mathbf{H}_x$ and $\mathbf{H}_y$. Among these Fourier components, only the ones with their reciprocal vectors located on the Ewald sphere participate in the transmission process, because it is these reciprocal vectors that make couplings between each two of the diffracted waves. The other components in the Fourier expansion can be ignored. There are four such "effective" reciprocal vectors here, as shown in Fig. 1(c): $\mathbf{H}_x$, $\mathbf{H}_y$, $\mathbf{H}_x+\mathbf{H}_y$, and $\mathbf{H}_x-\mathbf{H}_y$. Their corresponding "effective" Fourier components, denoted by M_1, M_2, M_3, and M_4, respectively, are then the "index-modulation strengths" of this 2D optical superlattice [14]. Thus, the periodic $\epsilon(\mathbf{r})$ can always be written in the form

$$\epsilon(\mathbf{r})/\epsilon_v=1+M_1\cos(\mathbf{H}_x\cdot\mathbf{r})+M_2\cos(\mathbf{H}_y\cdot\mathbf{r})$$
$$+M_3\cos[(\mathbf{H}_x+\mathbf{H}_y)\cdot\mathbf{r}]$$
$$+M_4\cos[(\mathbf{H}_x-\mathbf{H}_y)\cdot\mathbf{r}]\ , \tag{3}$$

where ϵ_v is the mean linear dielectric constant of the medium and satisfies $\mu_0\epsilon_0\epsilon_v=(k_v/\omega)^2$ $(k_v=|\mathbf{k}_1|=|\mathbf{k}_2|=|\mathbf{k}_3|=|\mathbf{k}_4|)$.

The intensity-dependent dielectric nonlinearity can be described by the nonlinear polarization term

$$\mathbf{P}_{\mathrm{NL}}(\mathbf{r},t)=\epsilon_0\delta n(\mathbf{r},t)\mathbf{E}(\mathbf{r},t)\ . \tag{4}$$

Here, the nonlinear refractive index $\delta n(\mathbf{r},t)$ takes the Kerr form. Considering the relaxation of the nonlinearity [9,16], we assume that $\delta n(\mathbf{r},t)$ obeys the following Debye relaxation equation:

$$\tau\frac{\partial\delta n(\mathbf{r},t)}{\partial t}+\delta n(\mathbf{r},t)=\alpha|\mathbf{E}(\mathbf{r},t)|^2\ , \tag{5}$$

where τ is the relaxation time of the dielectric nonlinearity, and coefficient α characterizes the Kerr-form nonlinearity.

Because the nonlinear refractive index is determined by the intensity of the light field, which consists of four diffracted waves, it has a well-defined spatial distribution. The nonlinear refractive index affects the transmission process by perturbing the index-modulation strengths. It can be expressed as

$$\delta n(\mathbf{r},t)=\delta n_0+\delta n_1\cos(\mathbf{H}_x\cdot\mathbf{r})+\delta n_2\cos(\mathbf{H}_y\cdot\mathbf{r})$$
$$+\delta n_3\cos[(\mathbf{H}_x+\mathbf{H}_y)\cdot\mathbf{r}]$$
$$+\delta n_4\cos[(\mathbf{H}_x-\mathbf{H}_y)\cdot\mathbf{r}]\ . \tag{6}$$

Assuming the diffracted waves are polarized in the Z direction, and considering the geometry of the transmission shown in Fig. 1(b), we write the envelopes of the diffracted waves as

$$\mathbf{E}_i=E_i(x,t)\hat{\mathbf{k}}\quad(i=1,2,3,4)\ . \tag{7}$$

By applying the slowly varying envelope approximation and putting Eqs. (1), (3), (6), and (7) into Eq. (2), assuming $M_i,n_i\ll1$, we get the following coupled first-order partial differential equations governing the envelopes of the diffracted waves:

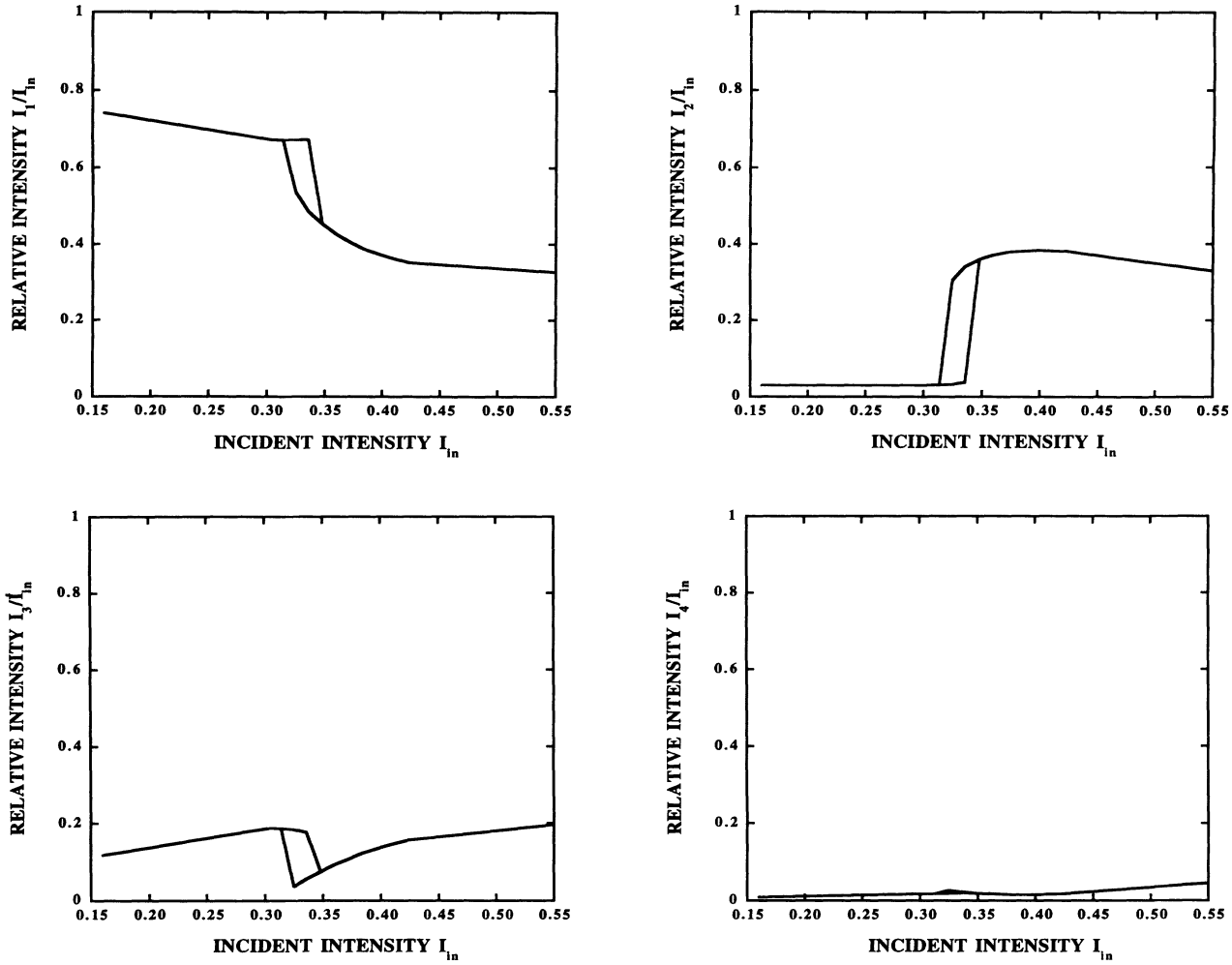

FIG. 2. Bistable behavior in the incident-diffracted relations obtained by time-independent numerical solution. The parameters are $M_1=3.0$, $M_2=6.5$, $M_3=M_4=0.1$, and $b=0.02$. I_{in} is measured in units of I_0, with $\alpha|E_0|^2=6\times10^{-3}$.

$$\frac{\sqrt{2}}{2}\frac{\partial E_1}{\partial x}+\frac{k_v}{\omega}\frac{\partial E_1}{\partial t}=\frac{k_v}{4i}[2\delta n_0 E_1+(M_2+\delta n_2)E_2+(M_3+\delta n_3)E_3+(M_1+\delta n_1)E_4]\,, \tag{8a}$$

$$\frac{\sqrt{2}}{2}\frac{\partial E_2}{\partial x}+\frac{k_v}{\omega}\frac{\partial E_2}{\partial t}=\frac{k_v}{4i}[(M_2+\delta n_2)E_1+2\delta n_0 E_2+(M_1+\delta n_1)E_3+(M_4+\delta n_4)E_4]\,, \tag{8b}$$

$$-\frac{\sqrt{2}}{2}\frac{\partial E_3}{\partial x}+\frac{k_v}{\omega}\frac{\partial E_3}{\partial t}=\frac{k_v}{4i}[(M_3+\delta n_3)E_1+(M_1+\delta n_1)E_2+2\delta n_0 E_3+(M_2+\delta n_2)E_4]\,, \tag{8c}$$

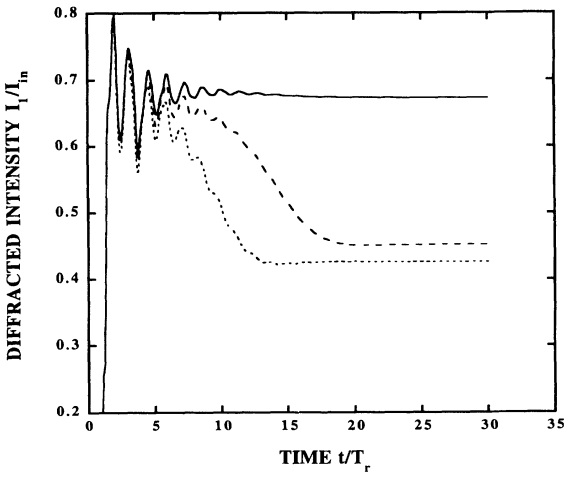

FIG. 3. Diffracted intensity I_1 as a function of time at three different inputs. Solid line, $I_{in}=0.58^2$; dashed line, $I_{in}=0.59^2$; and dotted line, $I_{in}=0.60^2$. The parameters are the same as those in Fig. 2.

$$-\frac{\sqrt{2}}{2}\frac{\partial E_4}{\partial x}+\frac{k_v}{\omega}\frac{\partial E_4}{\partial t}$$
$$=\frac{k_v}{4i}[(M_1+\delta n_1)E_1+(M_4+\delta n_4)E_2$$
$$+(M_2+\delta n_2)E_3+2\delta n_0 E_4]\ . \quad (8d)$$

By putting Eqs. (1), (6), and (7) into Eq. (5), we obtain the following material equations:

$$\tau\frac{\partial\delta n_0}{\partial t}+\delta n_0=\tfrac{1}{4}\alpha(|E_1|^2+|E_2|^2+|E_3|^2+|E_4|^2)\ , \quad (9a)$$

$$\tau\frac{\partial\delta n_1}{\partial t}+\delta n_1=\tfrac{1}{4}\alpha(E_1E_4^*+E_2E_3^*)+\text{c.c.}\ , \quad (9b)$$

$$\tau\frac{\partial\delta n_2}{\partial t}+\delta n_2=\tfrac{1}{4}\alpha(E_1E_2^*+E_3E_4^*)+\text{c.c.}\ , \quad (9c)$$

$$\tau\frac{\partial\delta n_3}{\partial t}+\delta n_3=\tfrac{1}{4}\alpha(E_1E_3^*)+\text{c.c.}\ , \quad (9d)$$

$$\tau\frac{\partial\delta n_4}{\partial t}+\delta n_4=\tfrac{1}{4}\alpha(E_2E_4^*)+\text{c.c.}\ . \quad (9e)$$

From the field equations in Eq. (8), we can see that the diffracted waves are coupled with one another by the index-modulation strengths through Bragg resonance. In the presence of the Kerr-form nonlinearity, the index-modulation strengths are subject to perturbations that depend on the strength of the light field. Consequently, the relative energy distribution among the four diffracted waves is dependent on the incident intensity.

The diffracted waves at their exit boundaries are determined by the field equations, the material equations, and the boundary and initial conditions $E_1(0,t)=E_{\text{in}}$, $E_2(0,t)=0$, $E_3(l,t)=E_4(l,t)=0$, and $E_i(x,0)=0$ $(i=1,2,3,4)$. Because of the complexity of these equations, even the steady-state solution $\partial/\partial t=0$ cannot be obtained analytically. We thus generally solve the equations by numerical methods, and treat the steady-state solution as a special case of the time-dependent solution.

III. NUMERICAL RESULTS

For convenience in the computations, we make the substitutions $\xi=x/l$ and $\eta=t/T_r$, where $T_r(=\sqrt{2}k_v l/\omega)$ is the transmission time of light through

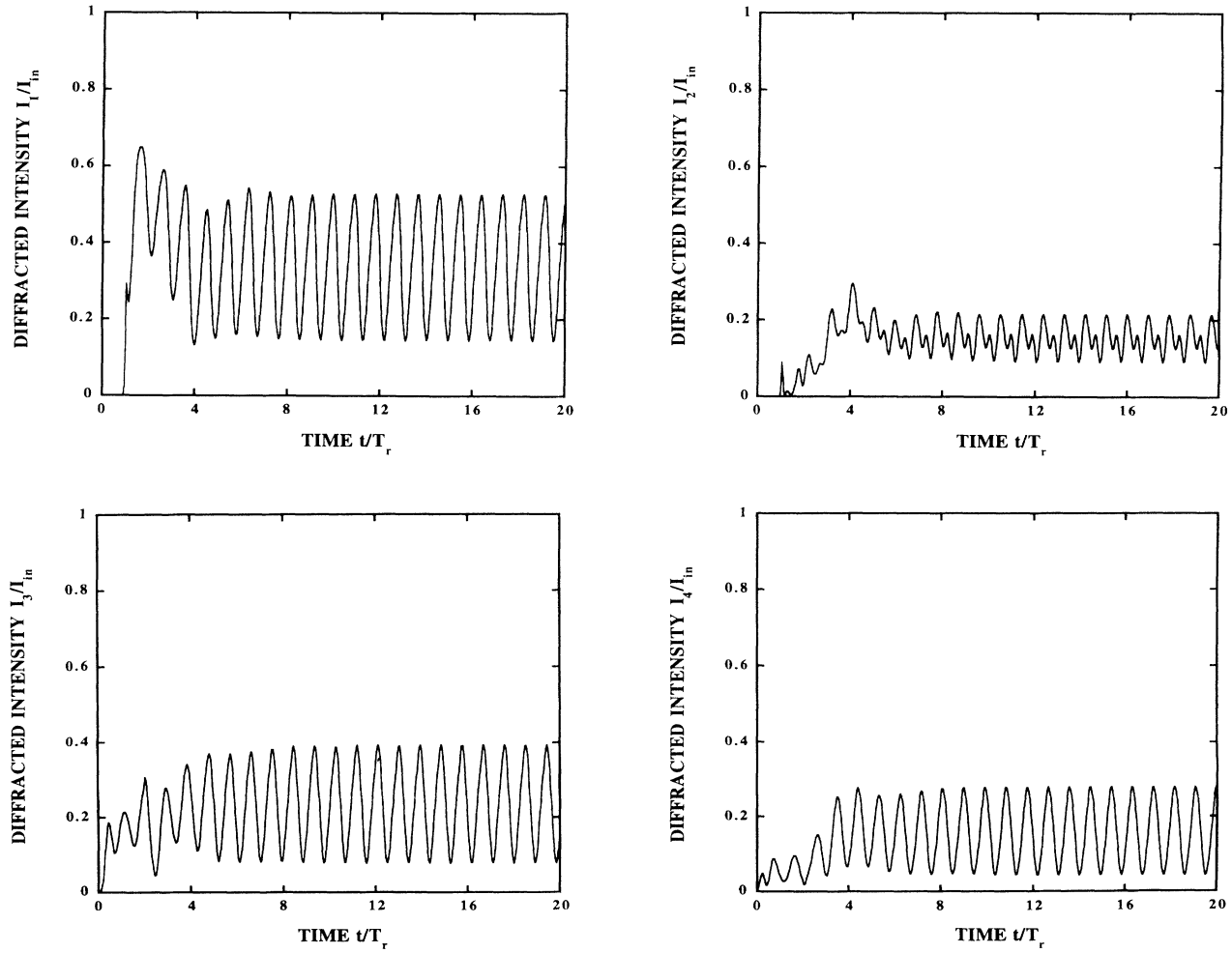

FIG. 4. Time-dependent solution showing periodic self-pulsing in the four diffracted waves, with $M_1=3.0$, $M_2=6.5$, $M_3=M_4=0.1$, and $b=0.02$. The incident intensity is $I_{\text{in}}=0.9^2$.

the superlattice. We also define $b(=\tau/T_r)$ to be the ratio of the relaxation time of the Kerr-form nonlinearity to the transmission time. To obtain sufficient high diffraction efficiency, the product M_i and the dimensionless constant $k_v l$ must be of the order of 1. In addition, the nonlinear index perturbation δn_i should be comparable to M_i, requiring the dimensionless constant $\alpha|E_0|^2$ to be of the same order of magnitude as M_i. Here E_0 is used to normalize the envelopes E_i of the diffracted waves. Since M_i is typical on the order of 10^{-3}, so should be δn_i. Thus in the following numerical computations, we assume, as an example, $k_v l=3\times10^3$ and $\alpha|E_0|^2=6\times10^{-3}$. With M_i and n_i measured in units of 10^{-3} and E_i in units of E_0, all the parameters appearing in the numerical computations are dimensionless and on the order of 1.

We notice that the first-order hyperbolic partial differential equations in Eq. (8) have the characteristics of straight lines. When using the standard finite-difference method to integrate the equations, we adopted the forward-backward (FB) finite difference form [17]. The grid size on the $\xi-\eta$ plane must be small enough so that convergence is achieved. With the boundary conditions and initial conditions, the envelopes of the diffracted waves at their exit boundaries are obtained. The numerical solution may be time-independent or time-dependent, and we present these two situations separately.

A. Time-independent solution

From the numerical results, we find that for low-incident amplitudes E_{in} (also measured in units of E_0), the solution will always evolve to a steady-state. From this stable solution, we can obtain the relationship between the incident intensity and the diffracted intensities. These functions of the diffracted versus incident intensities are nonlinear, as we have pointed out in Sec. II. However, what is of most concern here is whether bistable solutions can be obtained as expected. We have found that if the parameters of the superlattice such as the index-modulation strengths are suitably arranged, this bistable behavior is not difficult to obtain. Figure 2 shows bistability in the incident-diffracted relations. The bivalued region is obtained by changing the initial conditions. In single-valued regions, the steady solution is not

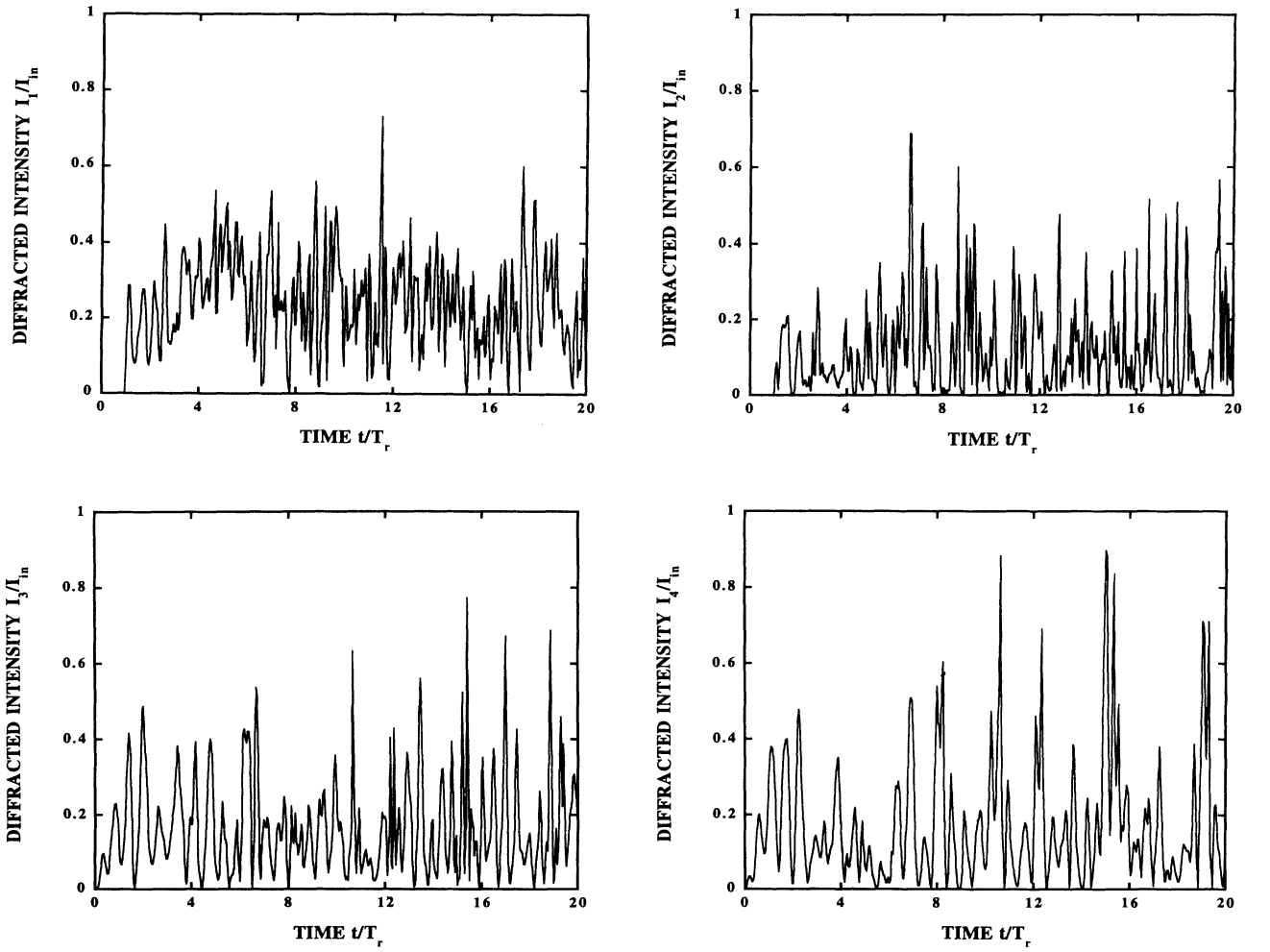

FIG. 5. Time-dependent solution showing chaotic behavior in the four diffracted waves with the same setting of parameters as that in Fig. 4. The incident intensity is $I_{\text{in}}=1.65^2$.

affected by changing the initial condition, whereas in the bivalued region, two solutions are achieved by having different initial conditions. To illustrate how the intensity jumps happen when changing the incident intensity slightly near the bistable domain, we plot in Fig. 3, for example, the variation of the intensity I_1 with time at three different incident intensities in the vicinity of a bistable jump. We can see that when I_{in} exceeds a critical value, the solution evolves in a different route and thus leads to a discontinuity in the diffracted intensity. This jump is always connected to the bivalued feature in our numerical computations, which is typical for bistable behavior.

As we mentioned in the Introduction, the bistability exhibited here corresponds to the transition between a low and a high transmission state in the allowed band [18]. This is indicated in Fig. 2. We can see that the two transmitted waves I_1 and I_2 jump in opposite directions. As the theoretical results show in Ref. [14], this behavior is connected only to oscillations in the allowed band, because no transmitted waves are permitted in the stop band. The perturbed index-modulation strengths and the transmission field are interacting with each other. Our results show that this kind of interaction can converge to a steady state only at low-incident intensities. When the incident power is high enough, the interaction is not stable and the solution will be time-dependent.

B. Unstable and chaotic solutions

When the incident intensity exceeds a threshold, we find that the numerical solution does not settle down to a fixed value but will keep oscillating with time. We plot in Fig. 4 this periodic self-pulsing behavior of the diffracted waves. The pulsation period is on the order of the transmission time T_r. At higher incident intensities, the numerical results reveal that this instability will eventually develop into chaos, as is illustrated in Fig. 5.

The route through which this nonlinear system enters chaos is intermittence [19]. The details are shown in Fig.

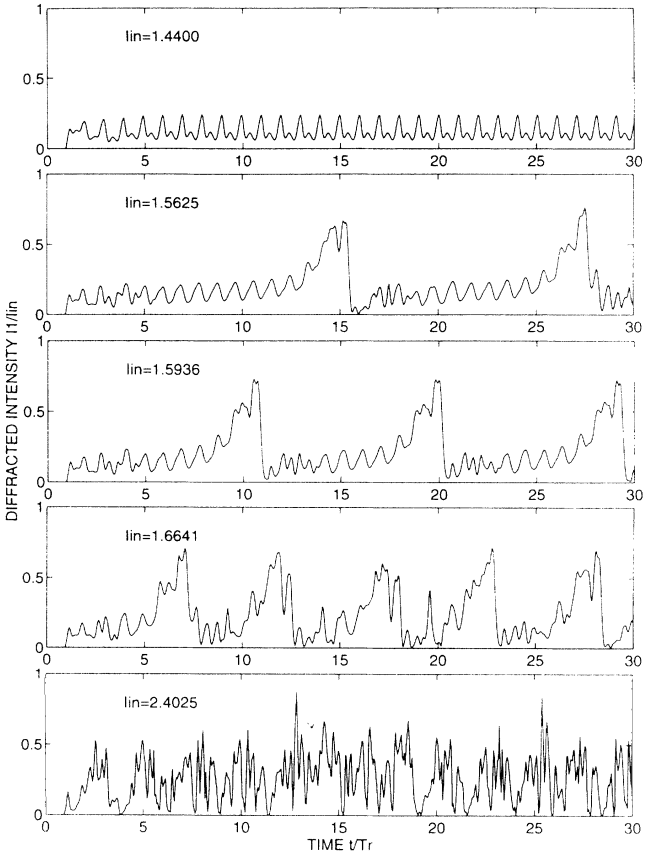

FIG. 6. Route of intermittence through which the system enters chaos, with $M_1=2.7$, $M_2=4.0$, $M_3=M_4=0.1$, and $b=0.02$.

6. With increasing incident intensity, the regular periodic self-pulsing becomes interrupted by irregular motions with statistically distributed periods. The average number of these intermittence bursts increases with the incident intensity until the condition becomes completely chaotic. It should be pointed out that in 1D optical su-

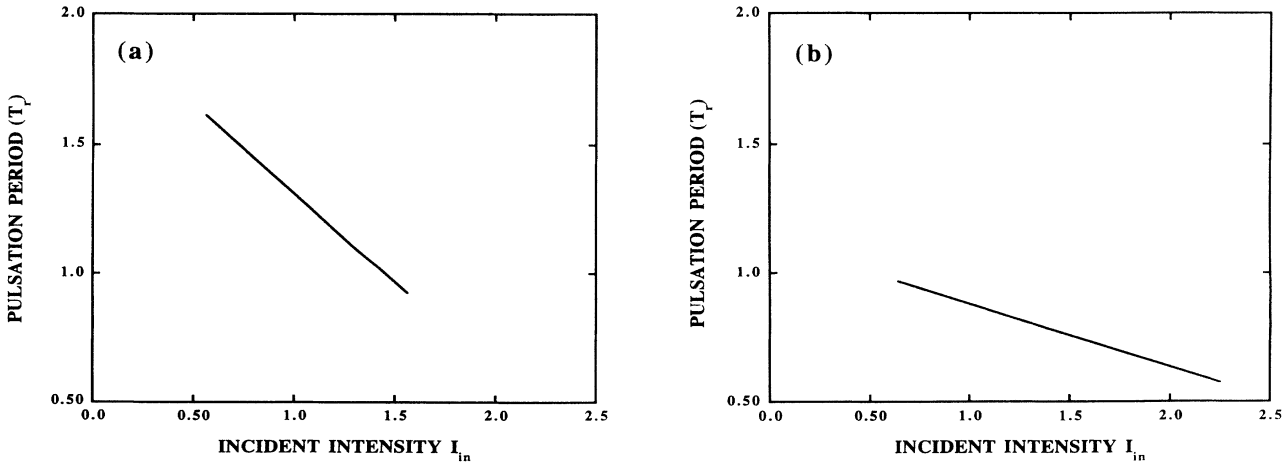

FIG. 7. In the region of periodic self-pulsing, plots showing the relationship between the pulsation period and the incident intensity. (a) $M_1=2.7$, $M_2=4.0$, $M_3=M_4=0.1$, and $b=0.02$. (b) $M_1=3.0$, $M_2=6.5$, $M_3=M_4=0.1$, and $b=0.02$. I_{in} is measured in units of I_0, with $\alpha|E_0|^2=6\times10^{-3}$.

perlattices, similar unstable behavior, such as self-pulsing and chaos, was also observed [9], but the route through which the system enters chaos is period-doubling bifurcations (see Ref. [11]).

In the region of the periodic self-pulsing, the pulsation frequency also increases with the incident intensity. We plot in Fig. 7 the relationship between the pulsation period and the intensity I_{in}, and find that this relation is approximately in a linear form.

The threshold in the incident intensity at which the system enters periodic self-pulsing or chaos is strongly dependent on the structural parameters, i.e, the index-modulation strengths. For example, for $M_1=2.7$, $M_2=4.0$, and $M_3=M_4=0.1$, the numerical solution shows that the incident intensity for the onset of periodic self-pulsing is $I_{in}=0.56$ and for the onset of chaos is $I_{in}=1.56$, while for $M_1=3.0$, $M_2=6.5$, and $M_3=M_4=0.1$, the two critical incident intensities for periodic self-pulsing and chaos are 0.64 and 2.25, respectively. We also notice (see Fig. 7) that, for the two sets of index-modulation strengths in (a) and (b), the slopes of the pulsation period versus incident intensity are different.

The instabilities we have discussed above are in the region $b=\tau/T_r \ll 1$. However, if τ is large enough to be comparable to T_r, we find that instabilities such as periodic self-pulsing or chaos are diminished. Instead, only time-independent solutions are obtained for any incident intensity. This situation is illustrated by the example of Fig. 8. The sluggish nonlinearity cannot provide instantaneous feedback and the pulses are washed out. This behavior is similar to that reported in a 1D superlattice (see Ref. [9]).

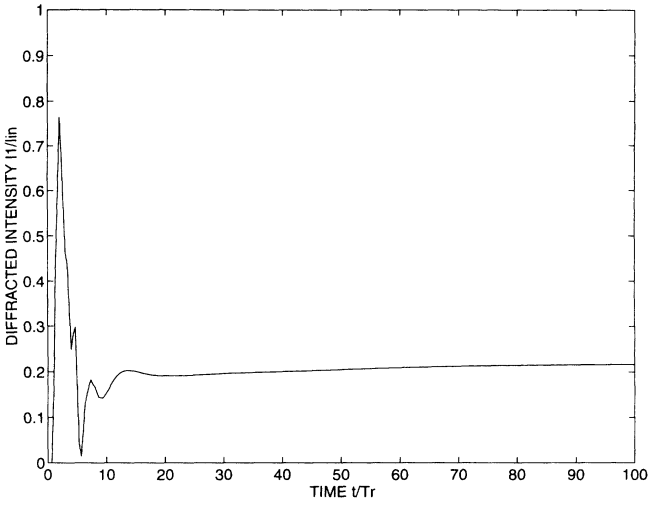

FIG. 8. The diffracted intensity as a function of time for a large relaxation time of $b=5.0$, with $M_1=3.0$, $M_2=6.5$, $M_3=M_4=0.1$, and $I_{in}=1.65^2$. The stable solution is obtained instead of the unstable solution with a small b of 0.02 in Fig. 5.

IV. DISCUSSION AND CONCLUSION

We have presented the numerical results showing the dynamics of light transmission in a 2D nonlinear superlattice, including stable and unstable cases. Similar behavior has also been investigated in 1D nonlinear superlattices [9,11]. However, the physical mechanisms operating in these two kinds of systems are not the same. As we have mentioned above, the perturbed index-modulation strengths play a key role in establishing bistability and unstable behavior in a 2D superlattice. That is to say, for a given cw radiation, the way in which the system works is dependent on the arrangement of the index-modulation strengths. The values of these parameters will determine whether the feedback is positive or negative. Based on the physical picture of the relationship between the transmission field and the index-modulation strengths that we have constructed in Ref. [14], the diffracted intensities are oscillatory functions of the index-modulation strengths. Thus, when the perturbations to these parameters, brought by the interference field via Kerr-form nonlinearity, are first enhanced with a small increase of the incident radiation, there is an organized trend in changing the energy distribution among the four diffracted waves. Radiation is increased in some diffracted directions and decreased in the others. Again via Kerr-form nonlinearity, there also appears a trend in the changes of the perturbations in the index-modulation strengths. This trend may favor the original trend in changing the field, or it may not, corresponding to positive feedback or negative feedback. Because of the oscillatory dependence of the transmission field on the index-modulation strengths, the positive feedback cannot last and will stop to change its sign at the peaks or valleys of the oscillations, leading to pulsed output of the diffracted waves with time in both stable and unstable numerical solutions. In the stable condition, the pulsation damps to zero, leaving the feedback negative, whereas for unstable conditions, such as periodic self-pulsing and chaos, the feedback is positive and is only interrupted by points at which it is negative. For bistable behavior of the stable solution, the jump should correspond to a range in which the feedback can always stay positive. It is obvious that the time-evolution of the feedback is determined by the values of the index-modulation strengths. We can divide M_1, M_2, M_3, and M_4 space into stable regions and unstable regions. Further quantitative analysis of this space remains to be made and is not covered by this paper. This division also depends on the incident power. As high-strength light transmission in a 2D superlattice causes the index-modulation strengths to variate over a broader range, the stable regions in M_i-space thus become smaller. The system can be located in unstable states by increasing the incident intensity.

As an application of this mechanism in 2D superlattices, for example, if the superlattice's periodic refractive index is introduced by the acousto-optic effect, then the index-modulation strengths will be determined by the acoustic field. At a fixed incident power, this system can work in a bistable state, a periodic self-pulsing state, or a chaotic state with different acoustic fields, and the periodic self-pulsing frequency can be controlled by the strength of the acoustic field.

ACKNOWLEDGMENTS

We thank Professor X. X. Yao for useful discussions and Professor T. A. B. Kennedy for helpful comments. This work is supported by a grant for the Key Research Project in Climbing Program from the State Science and Technology Commission of China.

[1] See, for example, H. M. Gibbs, *Optical Bistability: Controlling Light with Light* (Academic, New York, 1985).
[2] H. G. Winful, J. H. Marburger, and E. Garmire, Appl. Phys. Lett. **35**, 379 (1979).
[3] F. Delyon, Y. E. Levy, and B. Souillard, Phys. Rev. Lett. **57**, 2010 (1986).
[4] L. Kahn, N. S. Almeida, and D. L. Mills, Phys. Rev. B **37**, 8072 (1988).
[5] W. Chen and D. L. Mills, Phys. Rev. B **35**, 524 (1987).
[6] J. Danckaert *et al.*, Phys. Rev. B **44**, 8214 (1991).
[7] V. M. Agranovich, S. A. Kiselev, and D. L. Mills, Phys. Rev. B **44**, 10 917 (1991).
[8] J. He and M. Cada, IEEE J. Quantum Electron. **27**, 1182 (1991).
[9] H. G. Winful amd G. D. Cooperman, Appl. Phys. Lett. **40**, 298 (1982).
[10] P. A. Gohman, G. Bambakidis, and R. J. Spry, J. Appl. Phys. **67**, 40 (1990).
[11] C. M. de Sterke and J. E. Sipe, Phys. Rev. A **42**, 2858 (1990).
[12] H. M. Winful, R. Zamir, and S. Feldman, Appl. Phys. Lett. **58**, 1001 (1991).
[13] D. L. Mills and S. E. Trullinger, Phys. Rev. B **36**, 947 (1987).
[14] B. Xu and N. B. Ming, Phys. Rev. Lett. **71**, 1003 (1993).
[15] B. Xu and N. B. Ming, Phys. Rev. Lett. **71**, 3959 (1993).
[16] K. Ikeda, H. Daido, and O. Akimoto, Phys. Rev. Lett. **45**, 709 (1980); K. Ikeda and O. Akimoto, *ibid.* **48**, 617 (1982).
[17] L. Lapidus and G. F. Pinder. *Numerical Solution of Partial Differential Equations in Science and Engineering* (Wiley, New York, 1982).
[18] We do not exclude the possible bistability in 2D superlattices related to transmission transition between a forbidden state and an allowed state, but in this paper, we do not address this problem.
[19] R. G. Harrison and D. J. Biswas, Nature (London) **321**, 394 (1986).